Alan Ryder ORCID iD: 0000-0002-3133-4340

Analyzing protein conjugation reactions for Antibody-Drug Conjugate synthesis using polarized Excitation Emission Matrix spectroscopy.

Ana Luiza de Faria e Silva[1] and Alan G. Ryder.[1*]

[1]Nanoscale BioPhotonics Laboratory, School of Chemistry, National University of Ireland, Galway, Galway, H91 CF50, Ireland.

* To whom all correspondence should be addressed.

Tel: +353 91 49 2943; Fax: +353 91 49 5576 Email: alan.ryder@nuigalway.ie (A.G.R)

Grant number: 14/IA/2282, Advanced Analytics for Biological Therapeutic Manufacture, Science Foundation Ireland (SFI) with co-funding under the European Regional Development Fund.

Running Title: ADC reaction monitoring by polarized fluorescence spectroscopy.

Abstract

Antibody-drug Conjugates (ADCs) are promising anticancer therapeutics, which offer important advantages compared to more classical therapies. There are a variety of ADC Critical Quality Attributes (CQAs) such as the protein structure, aggregation, and drug-to-antibody ratio (DAR), which all impact on potency, stability, and toxicity. Production processes can destabilize antibodies via a variety of physical and chemical stresses, and via increased aggregation after conjugation of hydrophobic drugs. Thus, a proper control strategy for handling, production, and storage is necessary to maintain CQA levels, which

This article has been accepted for publication and undergone full peer review but has not been through the copyediting, typesetting, pagination and proofreading process, which may lead to differences between this version and the Version of Record. Please cite this article as doi: 10.1002/bit.28229.

requires the use of in-process quality measurements to first identify, then understand, and control the variables which adversely affect ADC CQAs during manufacturing.

Here we show how polarized Excitation Emission Matrix (pEEM), a sensitive, non-destructive, and potentially fast technique, could be used for rapidly assessing aggregation and DAR in a single measurement. pEEM provides several sources of information for protein analysis: Rayleigh scatter for identifying aggregate/particle formation and fluorescence emission to assess chemical and structural changes induced by attachment of a linker and/or a small molecule drug payload. Here we used a non-toxic ADC mimic (monoclonal antibody with linker molecule) to demonstrate efficacy of the measurement method. Emission changes caused via light absorption by the attached linker, allowed us to predict DAR with good accuracy using fluorescence signal from the final purified products (6% relative error of prediction (REP)) and also from unpurified alkylation intermediates (11% REP). pEEM changes could also be correlated with size (hydrodynamic radius, R_h) and aggregate content parameters obtained from Dynamic Light Scattering and Size Exclusion Chromatography (SEC). For the starting material and purified product samples, pEEM correlated better with R_h (R^2 =0.99, 6% REP) than SEC determined aggregate content (18% REP). Combining both fluorescence and light scatter signals also enabled in-process size quantification (6% REP). Overall, combining polarized measurements with EEM and Rayleigh scatter provides a single measurement, multi-attribute test method for ADC manufacturing.

Graphical Abstract

Spectroscopic monitoring of Antibody Drug Conjugate (ADC) synthesis can be challenging due to spectral overlap between reactants and products, and because of the need to simultaneously measure multiple process parameters. Here the authors show how polarized

Excitation Emission Matrix (pEEM) can rapidly assess aggregation and quantify the drug to antibody ratio via a single parallel polarised EEM measurement. pEEM is thus a potential Process Analytical Technology for real time reaction monitoring of ADC production

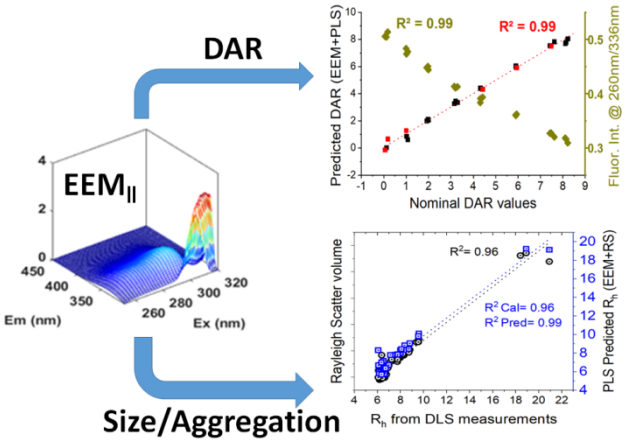

Keywords: Antibody Drug Conjugate, monoclonal antibody, conjugation, Fluorescence, Polarized.

1.0 Introduction

Antibody-drug conjugates (ADCs) couple the specificity of monoclonal antibodies (mAb) with the cell-killing ability of cytotoxic agents. This is done to increase specificity towards tumor cells as well as improving pharmacokinetic profiles, and providing a wider therapeutic window (Wu & Senter, 2005). There are currently nine FDA approved ADCs with more than 80 molecules in clinical studies (Joubert et al., 2020). IgG1 is the most widely used antibody type for therapeutic purposes and also the most common protein found in ADCs on the market or in late stage clinical trials (Joubert et al., 2020). Chemical conjugation via lysine and cysteine are the most common ADC synthetic strategies (Joubert et al., 2020). Conjugation to lysine amine group is widely used because it is relatively simple, often a single step reaction. However it generates heterogeneous products because IgG has approximately 80 lysine derived amine groups

(Mueller et al., 1988) of which approximately 10 are readily accessible for chemical modification. Cysteine conjugation is the major alternative, but because of the lack of free cysteine thiol groups in most proteins, the process usually first involves disulphide bond reduction under carefully controlled conditions to create sulfhydryl groups. These free thiols are then available for conjugation to reagents containing groups like maleimide. This route usually restricts the attachment sites to eight, leading to more homogeneous product mixtures compared to lysine conjugation (Jain et al., 2015), although site specific conjugation methods are now becoming available(Coumans et al., 2020).

Mishandling of proteins can lead to protein unfolding and aggregation, which can cause a loss in function and potentially cause immunogenicity issues for the patient (Sharma, 2007). In general, the most important critical quality attributes (CQAs) to be considered during protein modification are: homogeneity, purity, degree of conjugation, total protein concentration, and lot-to-lot variability of starting materials, intermediates, and final conjugated products. The CQAs ("Guidance for industry: Q8 (R2) pharmaceutical development, Guideline ICH Harmonised Tripartite," 2009) are the physical, chemical, or biological attributes of the drug substance/product known to impact product quality in terms of potency, pharmacokinetics, and toxicity(Alt et al., 2016; Raynal et al., 2014; Wagh et al., 2018). Protein and ADC analysis is technically demanding because of increased structural complexity compared to small molecules and the need to monitor both tertiary and quaternary structures. For ADC's, the problems are compounded by the fact that the small molecule payload also has to be characterized and

that the structural changes caused by the payload (e.g., increased hydrophobicity) lead to products which are significantly more sensitive to aggregation.

Using intrinsic fluorescence measurements for protein structure and stability analysis is well established, because it involves minimal structural perturbation compared to the use of extrinsic labels, and is sufficiently sensitive ($<10^{-6}$ M)(Quinn et al., 2015; Yadav et al., 2014). Simple (*i.e.* single point or single excitation measurements) intensity, lifetime, and anisotropy measurements can be implemented using relatively simple and inexpensive instrumentation and are widely used for studying processes like: aggregation (Ohadi et al., 2015), fibrillation (Bekard & Dunstan, 2009), unfolding (Vlasova & Saletsky, 2009), and binding.(Lissi et al., 2013; Rawel et al., 2006; Soares et al., 2007; Zhang et al., 2008) However, most proteins are multi-fluorophore systems with photophysically active species present in close proximity (<10 nm) which interact via energy transfer and quenching. This generates complex emission which is better represented by 3D measurements like Excitation Emission Matrix (EEM)(Warner et al., 1977) or total synchronous fluorescence spectroscopy, (TSFS) (Patra & Mishra, 2002). Both have been used for multi-fluorophore mixture analysis for various applications (Bridgeman et al., 2011; Li et al., 2011; Li et al., 2014; Ryan et al., 2010). By combining polarization with 3D EEM measurements, one can obtain extra information about changes in molecular size, local viscosity, and/or fluorophore mobility (Casamayou-Boucau & Ryder, 2017; Groza, 2016; Groza et al., 2015).

Here we investigated the use of polarized EEM (pEEM) to monitor an ADC reaction process with the key objectives being to: 1). measure variance in the mAb starting reaction materials, 2). monitor the course of the reaction and assess variance in the

reaction intermediates, 3). predict final product drug to antibody ratio (DAR) during the alkylation reaction, and 4). measure variance and DAR of the final purified products. Most ADCs analysis studies focus on characterizing final conjugate stability and DAR (Wakankar et al., 2011) with fewer looking at conjugation reaction monitoring. UV-vis absorbance spectroscopy (Andris et al., 2018) was used to monitor DAR during conjugation of two different drug mimics to an engineered mAb. A RP-HPLC and TOF mass spectrometry based method (Tang et al., 2017) was used to monitor DAR of a randomly conjugated lysine linked ADC. Our work presents a very different, multi-attribute alternative for assessing aggregation changes during the reactions, measuring DAR during alkylation, and DAR in the final, partially purified product.

2. Materials and methods

Materials: mAb donated by Byondis (Nijmegen, NL) was buffer exchanged prior to use (*vide infra*), MC-Val-Cit-PAB-OH linker was purchased from Tokyo Chemical Industry, and TCEP hydrochloride, n-acetylcysteine, and reagents for buffer preparation (NaH_2PO_4, $Na_2HPO_4{*}7H_2O$ and disodium EDTA dehydrate) were purchased from Sigma-Aldrich. HPLC grade water (Fisher chemicals) was used for all solutions which were membrane filtered (0.10 μm) using Captiva Filters prior to use. A single 11.0 mL mAb aliquot (see Supplemental Information, SI, for more details) was buffer exchanged to remove the formulation buffer in order to facilitate synthesis. The mAb in reaction buffer was then aliquoted into smaller vials (5.0 mL LoBind tubes) suitable for single experiments, refrozen, and stored at –70°C until required. This reduces and controls the number of freeze thaw cycles ensuring that all samples in an experimental campaign have the same number of cycles. Absorbance spectroscopy was used to check the final

concentration (of mAb in PBS/EDTA and fluorescence measurements and dynamic light scattering (DLS) were also carried out (data not shown). Ellman's test (Figure S1, Table S1, SI) was used to verify the number of free thiol sites under the different conditions employed.

Linker and Conjugation: A big challenge when studying ADCs is the often very high potency of the payload drug requiring the use of strict safety protocols and controlled environments. Thus, the safest alternative for preliminary studies particularly for analytical method development is to use a non-toxic model with payload molecules that mimic the structure/behavior of the real drug-linker which facilitates the safe study of all the key steps from starting material preparation to final purification of conjugated products. The drug mimic used here was selected to be similar (e.g., solubility, absorptivity) to common drug-linkers used in marketed ADCs but avoided toxicity issues. We used a molecule composed of valine, citruline, PAB-OH, with an active maleimide terminal group, which is a common commercial ADC linker (Joubert et al., 2020). We selected a non-fluorescent small molecule because we wanted to minimize interference, and only measure the changes in protein fluorescence (Figure S2/S3, SI).

Conjugates were prepared by partial reduction of IgG disulphide bonds with TCEP.HCl for 2 hours followed by alkylation with an excess of the "drug" linker for 2 hours, at 20°C. The two-step reactions were conducted in 1×1cm path length quartz cuvettes with slow stirring (using a flea magnetic follower in the cuvette with the sample holder stirrer) in the spectrometer (Figure S3, SI). A total of 24 reactions were performed, using 8 reducing agent TCEP concentrations from 0 to 50 molar excess (0, 1.25, 2.50, 5.0, 7.5, 10, 25, and 50) in triplicate. For all reactions, the same amount of "drug" linker

(20-fold excess compared to mAb concentration) and NAC quencher (12-fold excess with respect to linker concentration) was used. The reaction mixtures were measured by absorbance and pEEM spectroscopy at 45-minute intervals during the reaction (designated Red1-/2-/3-IgG, Alk1-/2-/3-/4-IgG). The starting material (IgG-SM), reduced intermediate (Red3-IgG), unpurified final reaction mixture (Alk4-IgG), and partially purified final products (Pur-ADC) were also analyzed by DLS to look for aggregate formation (See Tables S2/S3, SI). Because DLS, absorbance, and fluorescence measurements were made on the same cuvette sample we have confidence that all data relates to the exact same sample in terms of chemical and physical composition. Unpurified reaction mixtures were transferred to Eppendorf tubes and then stored at –70°C until purification was undertaken, several days post reaction. A simple filtration-based purification (see SI) was implemented to remove unreacted small molecules (<10kDa) and these partially purified samples (Pur-ADC) were characterized by absorbance and fluorescence spectroscopy, DLS, SEC, and Sodium Dodecyl Sulfate-Polyacrylamide gel electrophoresis (SDS-PAGE).

Instrumentation and data collection: Absorbance spectra were collected using a Cary 60 spectrometer (Agilent) from the same cuvettes used for fluorescence measurements. Polarized EEM spectra were collected from 1×1 cm quartz cuvettes (Lightpath Optical, UK) using a Cary Eclipse fluorescence spectrophotometer (Agilent) fitted with wire grid polarizers (Casamayou-Boucau & Ryder, 2017) and a temperature controlled multi-cell holder. pEEM spectra were collected over an excitation range of λ_{ex} = 250–320 nm and an 290–450 nm emission range (2 nm increments in each case) with 10 nm excitation/emission slit widths and a scan rate of 1200 nm/min. Samples were

measured under the four different polarization configurations, as previously described (A.L de Faria e Silva et al., 2020; A. L. de Faria e Silva et al., 2020), but only the parallel polarized EEM ($EEM_{\parallel}$) was used here because it is more sensitive to changes induced by conjugation and aggregation.(A.L de Faria e Silva et al., 2020; A. L. de Faria e Silva et al., 2020), and does not need G factor correction, simplifying measurement. Data were blank subtracted prior to any data analysis using the corresponding buffer for each step (see SI). pEEM data was corrected for differences in instrument response using a correction factor calculated using a Spectral Fluorescence Standard Kit (Sigma, product No. 69336) (Resch-Genger et al., 2005), for a restricted λ_{em}=302–450 spectral range (this was because the standards only covered the 300-700 nm emission range). Following this, the Rayleigh scatter (RS) area was replaced with missing data, and the fluorescence signal smoothed using Savitzky–Golay filter. For most analyses, the smoothed spectra were normalized to the point of the maximum intensity. The extracted RS band ($RS_{\parallel}$) is the first order Rayleigh scattering spectrum, and from this the area under the curve (RS volume) was calculated. Both of these parameters were used for qualitatively assessing protein aggregation. Descriptions of sample types, data collected, and datasets used for modelling are provided in Table S2, SI.

Chemometric analysis were performed using PLS_Toolbox 8.2.1®, MATLAB (ver. 9.1.0), and in-house written codes. Exploratory data analysis was carried out using ROBust Principal Component Analysis (ROBPCA), which minimizes the effect of outliers (Hubert et al., 2005) compared to classical PCA. It was implemented using the Venetian blind method (4 splits) for cross-validation and the Root Mean Square Error (RMSE) values to select the optimum number of PCs. Quantitative modelling for DAR

and % of aggregates was implemented using unfolded PLS, u-PLS, (Haaland & Thomas, 1988). Model performance was assessed by coefficient of determinations (R^2), RMSE, and relative error of prediction (REP). The elliptical joint confidence region (EJCR) test was used to compare the accuracy and precision of different models at a 95% confidence interval (Mandel & Linnig, 1957). iPLS was used for variable selection and it works by comparing u-PLS performance with and without each variable (here each excitation wavelength), selecting variables that return lower cross validation errors (Nørgaard et al., 2000). The pooled relative standard deviation (RSD_P) of SEC and DLS parameters was calculated using the RSD of values obtained from replicate measurements (see SI).

SEC was performed using a 300×7.8 mm mAb PAC-SEC. 1 column (ThermoFisher) with a 5µm particle size with an Agilent 1260 HPLC system equipped with a DAD detector. Solutions were filtered using a 0.20µm Captiva PES filter and 10µL of sample were injected in triplicate at 30°C with 50mM Sodium Phosphate pH 6.8+300 mM NaCl buffer as the mobile phase, and a 0.8 mL/min flow rate. The important output parameter used for characterization and modelling was the %Agg. value which for this study was defined as: the ratio in % terms of the sum of the Area Under the Curve (AUC) of the aggregate peaks (all those at Rt<10 minutes) divided by the total peak area in the SEC chromatograms. Because no fragment peaks were observed and the buffer components peak (~14 min) was excluded, the % of aggregates corresponded to 100_(% Monomers). Here the aggregate peaks occur between Rt=~7 and 10 min. However, we do have to note that the %Agg. values here represent the soluble species and do not take into account large aggregates which might precipitate out or otherwise be lost. DLS data were collected at 20 °C, after filtration (0.20µm PES filter), using a

Malvern Zetasizer Nano ZS (173°detection angle). Each sample was measured 5 times (each measurement was an average of 10 runs of 10 second duration) in disposable plastic cuvettes. Z-average size (radius) and Polydispersity Index (PdI) were obtained by Cumulants analysis while the hydrodynamic radius (R_h) was extracted from the distribution fit (both from the Intensity PSD), using the Zetasizer software, ver. 7.13 (Malvern Panalytical). SDS-PAGE was performed according to the BioRad TGX Precast Gels® specifications (see SI for details).

3. Results and discussion

Starting materials (IgG-SM) and partially purified products (Pur-ADC) were first characterized using conventional methods to measure aggregation by SEC, size by DLS, and DAR via UV-visible absorbance spectroscopy. This data was then used to explain the observed spectral changes in the pEEM spectra before using multi-variate data analysis to build predictive models for DAR and aggregation content.

3.1. Conventional reference measurements:

3.1.1 DAR quantification: As all reactions were undertaken in cuvettes, we expected high recovery, however, absorbance spectroscopy suggested a decrease in total protein concentration over the course of the reaction (Figure 1A). Average absorbances of 1.08±0.02 (IgG-SM), 1.04±0.01 (Red3-IgG), and 0.98±0.02 g/L (Alk4-ADC) were measured, with a decrease due mostly to dilution via reagent addition. Recovery after purification was ~75% which was a significant protein loss experienced during handling and reconstitution of purified material which is to be expected with the small reaction volumes used. The final purified solutions used for measurements had a concentration (measured by absorbance) of 1.05±0.02 g/L. DAR can be considered one of the most

important CQAs because it determines the final product potency and stability. Absorbance spectroscopy is often used to determine DAR if drug and mAb have different absorption maxima (Chen, 2013; Wakankar et al., 2011). However free drug is a problem if its absorbance spectrum overlaps that of the conjugated drug, which could lead to DAR overestimation. Here we collected absorbance spectra from the purification washings to ensure complete free "drug" removal. DAR was calculated from the ratio of the concentrations of "drug" and mAb (see SI) which were determined using the extinction coefficients at the two wavelengths of maximum absorbance (Hamblett et al., 2004). It confirmed that varying degrees of conjugation, 1.0±0.0 to 8.2±0.1 DAR (Table 1), were achieved. The maximum number of conjugation sites should be eight, however the slightly higher DAR value measured could be a result of small variations in protein absorption at 250–270 nm or possibly some conjugation to intra-chain disulphide bonds (which would result in more than eight free thiols and higher DAR).

3.1.2 Physical Characterization: SDS-PAGE gels indicated that all reactions were relatively clean, while also giving information about attachment sites within the antibody (**Figure 1**B). The rationale behind this is the dissociation of the antibody into light and heavy chains (L and H) which are no longer covalently attached via disulphide bonds (because of conjugation). With the increased TCEP (and thus higher DAR), the amount of unconjugated IgG (HHLL, 150kDa) decreased, with a concomitant increase in dissociated L (25kDa), H (50kDa), HL (75kDa), HH (100kDa), and HHL (125kDa) species depending on the degree of conjugation and site of attachment. This agreed with the claim that inter H-L di-sulphide bonds were the first reduced under mild reducing conditions (Guo et al., 2014). The gels also showed good reproducibility between

replicate experiments as demonstrated by the band patterns (Figure S4, SI). SEC-HPLC (Figure 1C) aggregation data and DLS (Figure 1D) R_h data (Table 1 and Table S3, SI) showed that all IgG-SM had very similar aggregation profiles (99.2±0.1 % monomer) and sizes. These measurements also showed that aggregation increased after purification (87.9±13.3 % monomer).

3.0 pEEM Measurements.

3.1 Fluorescence Spectroscopy: Normalized $EEM_{\parallel}$ difference spectra showed significant intensity changes (at λ_{ex}<260 nm) of up to 20% for the highest DAR samples (Figure 2A) which was probably related to secondary changes in fluorescence induced by varying Inner filter Effect (IFE) caused by light absorption by attached linker, rather than large changes in intrinsic protein emission. IFE is usually considered a problem because it causes a non-linear dependence between intensity and concentration. However, it is a valuable source of information about protein-based samples because of the high sensitivity to changes in sample composition (Panigrahi & Mishra, 2019; Ryder et al., 2017) and can be incorporated into variance assays once identified and taken into account.

To better interpret the spectral changes and their significance we used ROBPCA, which generates loadings plots to provide information about the types of spectroscopic changes occurring and scores plots that provide data on the magnitude/significance of these changes. ROBPCA of IgG-SM +Pur-ADC samples (

Table **3**, Figure 2B-C) easily discriminated conjugated from non-conjugated mAb with most separation along PC1 (78% explained variance) which is caused by spectral differences at $\lambda_{ex/em}$~260/340 nm due to increased absorbance by attached linker

molecules (λ_{max} = 250 nm) and a corresponding decrease in Trp emission as DAR increases due to IFE induced by linker attachment. PC2 (15.26%) represents changes centered at $\lambda_{ex/em}$~280/340 nm and seems to be related to changes in the directly excited intrinsic fluorophores (Trp and Tyr) but mostly Trp. Because PC2 scores decreased with DAR, this suggested some form of quenching via non-radiative transitions. PC3 (4.07%) seems to represent the intrinsic protein variance related to small variation in concentration (~2%) as sample distribution was linear along PC3 and the scores showed a negative signal at λ_{ex} ~300 nm with very little change at shorter excitation wavelengths. The fact that IgG-SM samples were distributed along PC3 also supports this view.

3.2 DAR quantification: Based on these observations, we built a u-PLS model (Table 2) for DAR quantification using the Pur-ADC normalized pEEM spectra (Figure 3A) with samples split into calibration and validation sets using the Kennard-Stone Algorithm. The best model obtained had relatively small error (RMSE<6%), and then by using iPLS variable selection, it was possible to reduce the number of excitation wavelengths, facilitating shorter acquisition times while maintaining similar prediction performance (REP=8%) as shown in the EJCR plot (Figure 3B). Both u-PLS selected variables and ROBPCA loadings (Figure 3C-E) indicated that two main spectral regions contributed to the quantification model, thus one can build a simpler, more transparent DAR correlation model using single data points, e.g., intensity at $\lambda_{ex/em}$ = 260/336 nm, or better use a ratio measurement between $\lambda_{ex/em}$ 260/336 and 292/336 nm. Both gave good correlations (R^2=0.99) with the nominal DAR. This demonstrates a key use of EEM measurements and chemometric analysis for quickly screening the full emission space to find simpler measurement options.

3.3 Aggregation Analysis and prediction: Aggregation is a critical CQA to be monitored during ADC production and it is thus important to monitor changes in both tertiary and quaternary structure. An increase in insoluble aggregates was indicated by a general rise in the ultraviolet aggregation index ($UV - AI = (A_{350}/(A_{280} - A_{350})) \times 100$), 0.61±0.43 → 1.35±0.58 → 1.96±0.76% for IgG-SM, Red-IgG, and Alk-IgG (average values for all samples, n=24), respectively (Wang & Roberts, 2010). After purification, UV-AI decreased to 0.72±0.15% which could be a result of either de-aggregation or more probably selective aggregate loss during purification, since recovery was only ~75% (e.g., sedimentation of large aggregates). All the individual reactions apart from the control show similar trends and the complete data is available in the SI (Table S5/Figure S9). Previously we showed (A. L. de Faria e Silva et al., 2020) that UV-AI had a poor relationship with SEC measured aggregation, which was probably due to its poor sensitivity for small soluble aggregates. Turbidity measurements (usually OD_{350nm}) have been used to monitor protein aggregation with stress conditions(Ross & Wolfe, 2016) Here, there was no correlation between UV-AI with either SEC or DLS R_h values (Figure 4A), which shows that UV-AI is unsuitable for this type of sample/process where relatively low levels of soluble aggregates are present. However, there was a good correlation (R^2>0.9, Table 1, plot not shown) between R_h and % aggregates for the Pur-ADC, which indicated that the issue for UV-AI was sensitivity. $RS_{\|}$ volume on the other hand, generated significantly better correlations to both R_h (DLS) and %Agg (SEC), R^2 =0.96 and 0.88 respectively (Figure 4B), for the combined IgG-SM and Pur-ADC sample set. Considerably lower correlations (R^2=0.44) were obtained for Z-average which was unsurprising since the Z-average size metric is

unreliable for polydisperse samples with PdI>0.1, (Bhattacharjee, 2016). Here all the Pur-ADC samples had PdI > 0.2. It is probably because of the ~30% (on average) R_h increase between IgG-SM to Pur-ADC (Table S3, SI) that we get good correlations with $RS_{\parallel}$ volume measurements. In cases where the distribution fits showed a second larger species, it was present only in relatively small quantities (<3% in the Pur-ADC) and as such seem to have a low influence on the model. However, these reference DLS size measurements need to be investigated further in future studies.

u-PLS predictive models (

Table **4**) for quantification/prediction of %Agg (SEC) and R_h (DLS) using $EEM_{\parallel}$ and $RS_{\parallel}$, showed that R_h prediction was better. This suggested that the presence of species which were not detected by SEC (e.g., non-covalent aggregates or very large particles), had a significant impact on $EEM_{\parallel}$ and $RS_{\parallel}$ spectra. Non-covalent aggregates could be either agglomerates or reversible aggregates, however, we have no data available to discriminate between the two. The higher errors obtained for %Agg prediction (REP>18%) can also be related to greater SEC measurement errors (RSD_P =4.2%) compared to DLS (2.3%). Other error factors were possible sample changes caused by an extra freeze-thaw cycle, additional sample handling, and the time delays making SEC measurements.

Aggregate content (%Agg. from SEC measurements) was better correlated to fluorescence than to scatter signals (but best when both signals were used), which was probably due to the weaker scatter contribution of the nm sized soluble aggregates (most samples were composed of monomers, dimers, and trimers according to SEC), and also because of the noisy/variable absolute scatter signal measured. This is clearly seen in

EJCR plots (Figure 4C) which confirmed that the model using both $EEM_{\parallel}$+$RS_{\parallel}$ data with variable selection was best. Here, with a relatively large sample set and using a mAb which better represents therapeutically relevant molecules, pEEM can be used for the quantification of soluble aggregates (as determined by SEC measurements) down to ~1% (

Table **4**) which is significantly better than demonstrated previously for a polyclonal IgG (A. L. de Faria e Silva et al., 2020).

pEEM spectral variance correlated better with R_h with the $RS_{||}$ based models being slightly better than those using $EEM_{\parallel}$ spectra (

Table **4**). The major issue with using non-normalized RS data for modelling aggregation was noise and poor reproducibility because the model relied on absolute intensity changes. We attempted to quantify aggregation using normalized $RS_{||}$ (by either band maximum or area), but this produced worse results (data not shown). Despite this, the error was relatively low and could be improved by spectral averaging. Another solution is to simply use normalized full pEEM spectra to minimize unwanted signal fluctuations (fluorescence and RS), which should be a more reproducible source of size related changes. Here, a specified spectral data point ($\lambda_{ex/em}$ 294/336nm, point of maximum fluorescence intensity) was used for normalization. Using this data resulted in better R_h models with good correlation coefficients (R^2>0.95) and a 2-3% decrease in REP for $EEM_{\parallel}$+$RS_{\parallel}$ compared to $RS_{\parallel}$. Larger improvements were obtained for aggregate content (

Table **4**) using $EEM_{\parallel}$+$RS_{\parallel}$, with R^2>0.98 and an REP decrease of 10-13%. iPLS selected variables and loadings (Figure S6) showed that areas of the fluorescence signal

and scatter band were important for size prediction of (Figure S6D/G/H) and aggregate content (Figure S6O/L/P), with the RS signal always being the strongest contribution. EJCR plots (Figure 4D) confirmed that the best model used both $EEM_{\|}$+$RS_{\|}$ data and variable selection.

4. Reaction monitoring:

4.1. Spectral changes: To investigate reaction dependent spectral changes, we collected pEEM spectra every 45 mins. during the reaction (nine measurements in total): one IgG starting material (IgG-SM), three during reduction (Red1/2/3-IgG), four during alkylation (Alk1/2/3/4-IgG) and one of the partially-purified product (Pur-ADC). The mean (

Figure **5**A-H) and standard deviation (StDev) spectra (

Figure **5**I-P) calculated from normalized spectra at each timepoint showed good reproducibility between IgG-SM (

Figure **5**A/E), and no major spectral changes during reduction (

Figure **5**B/F). Changes were more significant after linker addition (

Figure **5**C/G) and this carried through to the Pur-ADC (

Figure **5**D/H) although it was smaller presumably because the unreacted free drug had been removed. The relative standard deviation (RSD_{EEM}), see SI for explanation, for all starting materials (n=24) and all reduction intermediate samples (n=72) was 1.8%, with a maximum of 2% for a single data point, and a significantly higher variance amongst alkylation intermediates and purified product (EEM_{RSD}=8.8 & 4.4%, n=96 & 24 respectively). These were significant emission changes compared to 1% changes previously obtained for control measurements (A. L. de Faria e Silva et al., 2020). It was not possible to collect more spectra during the reaction because the scanning-based

spectrometer took ~7 min. to collect one full spectrum, which limited the number of sample points available for analysis and analysis of reaction rates.

We assessed the changes at each reaction step using StDev calculated after successively adding data collected at each data point e.g., for Step 3 of reduction StDev was calculated using IgG-SM + Red1-IgG + Red2-IgG + Red3-IgG samples (

Figure **5**). This again shows that alkylation was responsible for most of the reaction spectral variance, which increased from 8.2% to 11% (EEM_{RSD}) from the first to last sampling point. The equivalent variance (i.e., reproducibility), between replicates of same reaction at a specific timepoint, was much lower (<2%). Overall, we can say that the spectral changes induced by alkylation were large, significant, and thus suitable for ROBPCA and quantitative modelling (

Table 2).

ROBPCA (

Figure 6) was then used to better understand the source of these spectral changes and three ROBPCs were required to explain the spectral variance when models were built using all samples. This ROBPCA model contains more complex samples than that depicted in

Figure 2 and the presence of excess unbound linker had the largest impact. The outliers plot (

Figure **6**A) showed the significantly different samples and indicated some IgG-SM as outliers (bottom-right and top-left quadrants), but also some of the alkylation intermediates for reactions producing a lower DAR. The latter is probably associated

with changes in absorption/emission of free and linked drug, as there seem to be a decrease in Q Residuals with increasing DAR. The separation along PC1 (

Figure 6B) is largely associated with changes in emission induced by the presence of linker (

Figure 6C), which explained the separation of IgG-SM and Red-IgG groups from Alk-IgG (conjugated+free linker) and from Pur-ADC (varying DAR). ROBPC2, which only explained 1.20% of variance, represents a decrease in emission intensity, and thus probably represents small concentration and aggregate related variation arising from sample handling and other factors rather than significant structural change. This was because the tertiary structure of the starting material, reduced mAb, and the DAR 0 product should be similar. Thus, a global ROBPCA model containing all samples does not clearly show the reaction induced spectral changes very clearly.

The scores obtained for the two models (IgG-SM +Red-IgG and Alk-IgG) were plotted (Figure S7/8, SI) against reaction timepoint showing the trajectory followed by the different reaction conditions which lead to different DAR products. ROBPC1 and 2 of IgG-SM + Red-IgG indicated, as expected, very small changes in IgG emission during reduction, and highlighted the starting materials as the main sources of variation. Because the variance amongst IgG and Red-IgG was rather small (EEM_{RSD}<2%), it is possible that part of the changes modelled are related to instrument/measurement. For the alkylation process (Alk-IgG samples), PC2 showed the clearest correlation with DAR. It suggested (Figure S7F, SI) a possible combination of IFE at 310 nm and changes in Trp local environment (from less to more hydrophobic), with increasing DAR, which might

be associated with the amount of conjugated/free linker in solution which agreed with observations (

Figure 2).

We attempted DAR prediction using pEEM spectra collected during Alkylation, prior to purification (Table 2). Here absorbance spectroscopy was ineffective because of spectral overlap between free and conjugated linker, which resulted in very small spectral differences between in-reaction samples with different DAR (the same amount of linker was added to all reactions). u-PLS results suggested however, that there were small variances in pEEM spectra of the alkylation intermediates (Alk1–4), which correlated with DAR. Alk3-IgG had a better correlation with DAR (R^2>0.92, REP=11%) compared to Alk1/Alk2 because it was later in the reaction whereas the poorer correlation obtained with Alk4-IgG seems to be caused by interference from addition of the reaction quencher, NAC. When Alk1-4 absorbance spectra were used for DAR quantification, fairly good calibration results were obtained (Relative error of calibration, REC, =11%), but prediction errors were significantly worse (REP> 28%) compared to pEEM. Quantification here seems to be based on small absorbance changes at ~310 nm (and also IFE) due to loss of conjugation in the maleimide linker (–C=C–C=O→ –CH–CR–C=O) after alkylation (Liu et al., 2013), with the high quantification errors caused by increased scattered light at ~310 nm.

Overall, these results suggested that $EEM_{\|}$ was the better reaction monitoring option because of significant alkylation induced spectral changes. However, when we looked at the normalized score changes (Figure S8, SI) there was very little change from Alk1 to

Alk3 which suggests that alkylation was faster than anticipated and was nearly complete before the first pEEM measurement was completed.

4.2 Physical stability (in reaction): Previously we assessed polyclonal IgG solution quality using pEEM which indicated that most of the variance originated from longer wavelength emission (A. L. de Faria e Silva et al., 2020). Here, long wavelength emission did not play a role in discriminating solutions according to aggregation which suggested that the previous observations were related to lower purity and higher variability of polyclonal IgG. The emission ratio between solvent exposed and buried Trp residues (I_{350}/I_{330nm} using 296 nm excitation) is commonly used to assess protein stability (Beckley et al., 2013). Here the ratio did not correlate with R_h, which is clear evidence that there were no major structural changes like unfolding. As expected however, the reaction/purification did induce some physical sample changes as observed by DLS in the reported R_h (Table 1) and Z-average values (Table S3, SI).

Although disulphide bond reduction could increase flexibility, and linker addition causes a small increase in product mass (~3% for a DAR of 8) these did not cause large changes in the R_h values: R_h(IgG-SM)=6.4±0.3 nm, R_h(Red3)=6.1±0.1 nm, and R_h(Alk4)= 6.7±0.1 nm (Table S3, SI). However, there were very significant changes in derived count rates and PdI (~0.1 → ~0.5 → ~0.7 → ~0.2) and for IgG-SM, Red3-IgG, Alk4-IgG, and Pur-ADC, respectively (Table S3, SI). This suggested the formation of loosely bound reversible aggregates during the intermediate stages. After purification (Pur-ADC samples) R_h and variability (9.4±4.0 nm), increased, but there was also a significant drop in PdI compared to the intermediates. This indicated that the reversible aggregates formed earlier had broken down, and that the protein product may be somewhat

aggregated compared to the mAb starting material. This was probably due to reduced stability caused the attached hydrophobic small molecules and variable DAR, and/or via the stresses of purification and extra sample handling. Similar trends were observed with RS volume, but these had higher measurement error (Figure S5, SI). R_h and RS volume did not correlate (R^2<0.5) and, poor u-PLS regression results were obtained when using RS bands for size prediction.

While u-PLS results showed similar R_h prediction performance using IgG-SM and Pur-ADC samples ($EEM_{\parallel}$, $RS_{\parallel}$, and combined spectra), size prediction results were better when two other reaction samples (Red3-IgG, Alk4-IgG) were added to the model. This was probably due to a larger sample set size and greater protein size variability when these samples were included. Overall, use of full $(EEM+RS)_{\parallel}$ spectra enabled size prediction with low errors (REP<8%) and good correlation with nominal values (R^2_{Pred}=0.97), implying a more robust size change assessment for complex in-reaction samples.

4.3 Reaction End Point Determination: One goal of reaction monitoring is to accurately determine reaction end points, and this usually involves collecting multiple spectra throughout the reaction and then extracting kinetic and end-point data. Here, the long collections times coupled with the fast reaction kinetics, prevented this and thus we investigated a different approach. We used non-linear, Support Vector Machine (SVM) classification (Table S4, SI) to quantitatively assess if these low numbers of $EEM_{\parallel}$ measurements could classify samples according to reaction stage and the ultimate product DAR (i.e., predict end point for different performing reactions). Samples were split into calibration and validation sets and ten different classes were used for classification: IgG-

SM and reaction intermediates/Pur-ADCs from reactions producing low (1.0-2.0), medium (3.2-4.3), and high (5.9-8.2) DAR. The classification errors indicated a good performance for successfully classifying both reaction stages and DAR (errors lower than 10% for all the classes) for the medium and high DAR ranges. The low DAR related classes (and the IgG-SM) showed lower specificity, which was probably due to the very small spectral changes induced by the lower number of linker molecule attachments.

5.0 Conclusions

Using pEEM measurements for the non-destructive analysis of the key mAb linker reaction monitoring and product variance analysis has been demonstrated. Here, although the model reaction was limited to looking just at the linker addition, in small scale, and with insufficient time resolution, it does show the very significant spectral differences between each stage in the reaction process. Although spectral changes were relatively small (EEM_{RSD}=10 for all samples, n=216), they were significant and reproducible. By using the full pEEM spectral information, that is both the scatter and fluorescence signals, one is able to build quantitative models for predicting DAR using the alkylation intermediates (R^2>0.90 and REP 11%) and that correlate with aggregation and size (R_h, R^2_{PRED}=0.97 and REP=6%) parameters extracted from SEC and DLS measurements, respectively. We also showed that UV-AI measurements were poorly correlated with both %Agg. from SEC, and DLS derived size parameters, confirming its unsuitability for ADC reaction monitoring with these levels of soluble aggregates.

For reaction monitoring, the spectral profile changes observed here although small, were still significant considering that we only used normalized data. The u-PLS modelling showed that it was possible to generate in-process accurate correlations for

both size and aggregation parameters when using the combined scatter and fluorescence signals. For wider application using payload molecules with different absorption spectra that overlap less with the protein absorption spectra, and potentially more with protein emission spectra, we suggest that fluorescence spectral changes will be larger and thus easier modeled using these techniques. Larger signal changes should make DAR quantification and reaction monitoring easier to implement and potentially more accurate and this is the focus of future studies.

Although fluorescence and pEEM are not currently, widely used analytical techniques for monitoring ADC synthesis and manufacturing processes (it is mostly used to assess the effect of conjugation on higher order structure and stability (Turecek et al., 2016; Wakankar et al., 2011)), these results are very promising. However, this alkylation reaction was too fast for this spectrometer and was substantially complete by 10 minutes when the first in-process pEEM data was collected. For more accurate, continuous in-process monitoring we require either faster data acquisition using spectrometers with multichannel detectors or slower reactions, both of which are being investigated, along with the use of more therapeutically drug linker moieties. Overall, this use of the full pEEM measurement shows considerable promise as a robust PAT tool for ADC manufacturing.

Supplemental information available

Supporting information is available providing further details on the spectral and quantitative analyses.

Acknowledgements

This publication emanated from research supported in part by a Principal Investigator research grant (Grant Number 14/IA/2282) to AGR from Science Foundation Ireland and is co-funded under the European Regional Development Fund. We thank Agilent Technologies (Mulgrave Victoria, Australia) for a fluorescence spectrometer loan. Byondis (Nijmegen, the Netherlands), B. Kokke, and M. Eppink are thanked for the mAb donation and Daniel-Ralph Hermann for assistance with some experiments. The authors declare that there are no conflicts of interest.

Author contributions

Ana Luiza de Faria e Silva: conceptualization, designed and performed the experiments, analyzed the data, prepared all the figures, wrote, and edited the manuscript. Alan Ryder: conceptualization, supervision, funding acquisition, wrote and edited the manuscript.

References

Alt, N., Zhang, T. Y., Motchnik, P., Taticek, R., Quarmby, V., Schlothauer, T.,... Harris, R. J. (2016). Determination of critical quality attributes for monoclonal antibodies using quality by design principles. *Biologicals, 44*(5), 291-305. doi:https://doi.org/10.1016/j.biologicals.2016.06.005

Andris, S., Rudt, M., Rogalla, J., Wendeler, M., & Hubbuch, J. (2018). Monitoring of antibody-drug conjugation reactions with UV/Vis spectroscopy. *Journal of Biotechnology, 288*, 15-22. doi:10.1016/j.jbiotec.2018.10.003

Beckley, N. S., Lazzareschi, K. P., Chih, H. W., Sharma, V. K., & Flores, H. L. (2013). Investigation into Temperature-Induced Aggregation of an Antibody Drug Conjugate. *Bioconjugate Chemistry, 24*(10), 1674-1683. doi:10.1021/bc400182x

Bekard, I. B., & Dunstan, D. E. (2009). Tyrosine Autofluorescence as a Measure of Bovine Insulin Fibrillation. *Biophysical Journal, 97*(9), 2521-2531. doi:10.1016/j.bpj.2009.07.064

Bhattacharjee, S. (2016). DLS and zeta potential – What they are and what they are not? *Journal of Controlled Release, 235*, 337-351. doi:https://doi.org/10.1016/j.jconrel.2016.06.017

Bridgeman, J., Bieroza, M., & Baker, A. (2011). The application of fluorescence spectroscopy to organic matter characterisation in drinking water treatment. *Reviews in Environmental Science and Bio-Technology, 10*(3), 277-290. doi:10.1007/s11157-011-9243-x

Casamayou-Boucau, Y., & Ryder, A. G. (2017). Extended wavelength anisotropy resolved multidimensional emission spectroscopy (ARMES) measurements: better filters, validation standards, and Rayleigh scatter removal methods. *Methods Appl Fluoresc, 5*(3), 037001. doi:10.1088/2050-6120/aa7763

Chen, Y. (2013). Drug-to-Antibody Ratio (DAR) by UV/Vis Spectroscopy. In L. Ducry (Ed.), *Antibody-Drug Conjugates* (pp. 267-273). Totowa, NJ: Humana Press.

Coumans, R. G. E., Ariaans, G. J. A., Spijker, H. J., Renart Verkerk, P., Beusker, P. H., Kokke, B. P. A.,... Timmers, C. M. (2020). A Platform for the Generation of Site-Specific Antibody-Drug Conjugates That Allows for Selective Reduction of Engineered Cysteines. *Bioconjug Chem, 31*(9), 2136-2146. doi:10.1021/acs.bioconjchem.0c00337

de Faria e Silva, A. L., Elcoroaristizabal, S., & Ryder, A. G. (2020). Characterization of lysozyme PEGylation products using polarized excitation-emission matrix spectroscopy. *Biotechnology and Bioengineering, 117*(10), 2969-2984. doi:10.1002/bit.27483

de Faria e Silva, A. L., Elcoroaristizabal, S., & Ryder, A. G. (2020). Multi-attribute quality screening of immunoglobulin G using polarized Excitation Emission Matrix spectroscopy. *Analytica Chimica Acta, 1101*, 99-110. doi:10.1016/j.aca.2019.12.020

Groza, R. C. (2016). *Anisotropy Resolved Multi-dimensional Emission Spectroscopy (ARMES): A new tool for the quantitative and structural analysis of proteins. PhD thesis.* (Ph.D.), National University of Ireland Galway, Galway, Ireland.

Groza, R. C., Li, B. Y., & Ryder, A. G. (2015). Anisotropy resolved multidimensional emission spectroscopy (ARMES): A new tool for protein analysis. *Analytica Chimica Acta, 886*, 133-142. doi:10.1016/j.aca.2015.06.011

Guidance for industry: Q8 (R2) pharmaceutical development, Guideline ICH Harmonised Tripartite. (2009). *Current step, 4*.

Guo, J. X., Kumar, S., Prashad, A., Starkey, J., & Singh, S. K. (2014). Assessment of Physical Stability of an Antibody Drug Conjugate by Higher Order Structure Analysis: Impact of Thiol- Maleimide Chemistry. *Pharmaceutical Research, 31*(7), 1710-1723. doi:10.1007/s11095-013-1274-2

Haaland, D. M., & Thomas, E. V. (1988). Partial Least-Squares Methods for Spectral Analyses .1. Relation to Other Quantitative Calibration Methods and the Extraction of Qualitative Information. *Analytical Chemistry, 60*(11), 1193-1202. doi:DOI 10.1021/ac00162a020

Hamblett, K. J., Senter, P. D., Chace, D. F., Sun, M. M. C., Lenox, J., Cerveny, C. G.,... Francisco, J. A. (2004). Effects of drug loading on the antitumor activity of a monoclonal antibody drug conjugate. *Clinical Cancer Research, 10*(20), 7063-7070. doi:Doi 10.1158/1078-0432.Ccr-04-0789

Hubert, M., Rousseeuw, P. J., & Vanden Branden, K. (2005). ROBPCA: A new approach to robust principal component analysis. *Technometrics, 47*(1), 64-79.

Jain, N., Smith, S. W., Ghone, S., & Tomczuk, B. (2015). Current ADC Linker Chemistry. *Pharmaceutical Research, 32*(11), 3526-3540. doi:10.1007/s11095-015-1657-7

Joubert, N., Beck, A., Dumontet, C., & Denevault-Sabourin, C. (2020). Antibody-Drug Conjugates: The Last Decade. *Pharmaceuticals (Basel), 13*(9). doi:10.3390/ph13090245

Li, B., Ryan, P. W., Shanahan, M., Leister, K. J., & Ryder, A. G. (2011). Fluorescence excitation-emission matrix (EEM) spectroscopy for rapid identification and quality evaluation of cell culture media components. *Applied Spectroscopy, 65*(11), 1240-1249. doi:10.1366/11-06383

Li, B., Shanahan, M., Calvet, A., Leister, K. J., & Ryder, A. G. (2014). Comprehensive, quantitative bioprocess productivity monitoring using fluorescence EEM spectroscopy and chemometrics. *Analyst, 139*(7), 1661-1671. doi:10.1039/c4an00007b

Lissi, E., Calderon, C., & Campos, A. (2013). Evaluation of the Number of Binding Sites in Proteins from their Intrinsic Fluorescence: Limitations and Pitfalls. *Photochemistry and Photobiology, 89*(6), 1413-1416. doi:10.1111/php.12112

Liu, X. X., Du, P. F., Liu, L., Zheng, Z., Wang, X. L., Joncheray, T., & Zhang, Y. F. (2013). Kinetic study of Diels-Alder reaction involving in maleimide-furan compounds and linear polyurethane. *Polymer Bulletin, 70*(8), 2319-2335. doi:10.1007/s00289-013-0954-8

Mandel, J., & Linnig, F. J. (1957). Study of Accuracy in Chemical Analysis using Linear Calibration Curves. *Analytical Chemistry, 29*(5), 743-749. doi:10.1021/ac60125a002

Mueller, B. M., Wrasidlo, W. A., & Reisfeld, R. A. (1988). Determination of the number of e-amino groups available for conjugation of effector molecules to monoclonal antibodies. *Hybridoma, 7*(5), 453-456. doi:10.1089/hyb.1988.7.453

Nørgaard, L., Saudland, A., Wagner, J., Nielsen, J. P., Munck, L., & Engelsen, S. B. (2000). Interval Partial Least-Squares Regression (iPLS): A Comparative Chemometric Study with an Example from Near-Infrared Spectroscopy. *Applied Spectroscopy, 54*(3), 413-419. doi:10.1366/0003702001949500

Ohadi, K., Legge, R. L., & Budman, H. M. (2015). Intrinsic fluorescence-based at situ soft sensor for monitoring monoclonal antibody aggregation. *Biotechnology Progress, 31*(5), 1423-1432. doi:10.1002/btpr.2140

Panigrahi, S. K., & Mishra, A. K. (2019). Inner filter effect in fluorescence spectroscopy: As a problem and as a solution. *Journal of Photochemistry and Photobiology C: Photochemistry Reviews, 41*. doi:10.1016/j.jphotochemrev.2019.100318

Patra, D., & Mishra, A. K. (2002). Recent developments in multi-component synchronous fluorescence scan analysis. *Trac-Trends in Analytical Chemistry, 21*(12), 787-798. doi:Pii S0165-9936(02)01201-3

Doi 10.1016/S0165-9936(02)01201-3

Quinn, M. K., Gnan, N., James, S., Ninarello, A., Sciortino, F., Zaccarelli, E., & McManus, J. J. (2015). How fluorescent labelling alters the solution behaviour of proteins. *Physical Chemistry Chemical Physics, 17*(46), 31177-31187. doi:10.1039/c5cp04463d

Rawel, H. M., Frey, S. K., Meidtner, K., Kroll, J., & Schweigert, F. J. (2006). Determining the binding affinities of phenolic compounds to proteins by quenching of the intrinsic tryptophan fluorescence. *Molecular Nutrition & Food Research, 50*(8), 705-713. doi:10.1002/mnfr.200600013

Raynal, B., Lenormand, P., Baron, B., Hoos, S., & England, P. (2014). Quality assessment and optimization of purified protein samples: why and how? *Microbial Cell Factories, 13*. doi:ARTN 180

10.1186/s12934-014-0180-6

Resch-Genger, U., Pfeifer, D., Monte, C., Pilz, W., Hoffmann, A., Spieles, M.,... Nording, P. (2005). Traceability in fluorometry: Part II. Spectral fluorescence standards. *Journal of Fluorescence, 15*(3), 315-336. doi:10.1007/s10895-005-2629-9

Ross, P. L., & Wolfe, J. L. (2016). Physical and Chemical Stability of Antibody Drug Conjugates: Current Status. *Journal of Pharmaceutical Sciences, 105*(2), 391-397. doi:10.1016/j.xphs.2015.11.037

Ryan, P. W., Li, B., Shanahan, M., Leister, K. J., & Ryder, A. G. (2010). Prediction of Cell Culture Media Performance Using Fluorescence Spectroscopy. *Analytical Chemistry, 82*(4), 1311-1317. doi:Doi 10.1021/Ac902337c

Ryder, A. G., Stedmon, C. A., Harrit, N., & Bro, R. (2017). Calibration, standardization, and quantitative analysis of multidimensional fluorescence (MDF) measurements on complex mixtures (IUPAC Technical Report). *Pure and Applied Chemistry, 89*(12), 1849-1870. doi:https://doi.org/10.1515/pac-2017-0610

Sharma, B. (2007). Immunogenicity of therapeutic proteins. Part 1: Impact of product handling. *Biotechnology Advances, 25*(3), 310-317. doi:10.1016/j.biotechadv.2007.01.005

Soares, S., Mateus, N., & De Freitas, V. (2007). Interaction of different polyphenols with bovine serum albumin (BSA) and human salivary alpha-amylase (HSA) by fluorescence quenching. *Journal of Agricultural and Food Chemistry, 55*(16), 6726-6735.

Tang, Y. B., Tang, F., Yang, Y., Zhao, L., Zhou, H., Dong, J. H., & Huang, W. (2017). Real-Time Analysis on Drug-Antibody Ratio of Antibody-Drug Conjugates for Synthesis, Process Optimization, and Quality Control. *Scientific Reports, 7*. doi:10.1038/s41598-017-08151-2

Turecek, P. L., Bossard, M. J., Schoetens, F., & Ivens, I. A. (2016). PEGylation of Biopharmaceuticals: A Review of Chemistry and Nonclinical Safety Information of Approved Drugs. *Journal of Pharmaceutical Sciences, 105*(2), 460-475. doi:10.1016/j.xphs.2015.11.015

Vlasova, I. M., & Saletsky, A. M. (2009). Study of the Denaturation of Human Serum Albumin by Sodium Dodecyl Sulfate Using the Intrinsic Fluorescence of Albumin. *Journal of Applied Spectroscopy, 76*(4), 536-541.

Wagh, A., Song, H., Zeng, M., Tao, L., & Das, T. K. (2018). Challenges and new frontiers in analytical characterization of antibody-drug conjugates. *MAbs, 10*(2), 222-243. doi:10.1080/19420862.2017.1412025

Wakankar, A., Chen, Y., Gokarn, Y., & Jacobson, F. S. (2011). Analytical methods for physicochemical characterization of antibody drug conjugates. *Mabs, 3*(2), 161-172. doi:10.4161/mabs.3.2.14960

Wang, W., & Roberts, C. J. (2010). *Aggregation of therapeutic proteins*. Hoboken, N.J.: Wiley.

Warner, I. M., Christian, G. D., Davidson, E. R., & Callis, J. B. (1977). Analysis of Multicomponent Fluorescence Data. *Analytical Chemistry, 49*(4), 564-573.

Wu, A. M., & Senter, P. D. (2005). Arming antibodies: prospects and challenges for immunoconjugates. *Nature Biotechnology, 23*(9), 1137-1146. doi:10.1038/nbt1141

Yadav, R., Sengupta, B., & Sen, P. (2014). Conformational Fluctuation Dynamics of Domain I of Human Serum Albumin in the Course of Chemically and Thermally Induced Unfolding Using Fluorescence Correlation Spectroscopy. *Journal of Physical Chemistry B, 118*(20), 5428-5438. doi:10.1021/jp502762t

Zhang, G. W., Wang, A. P., Jiang, T., & Guo, J. B. (2008). Interaction of the irisflorentin with bovine serum albumin: A fluorescence quenching study. *Journal of Molecular Structure, 891*(1-3), 93-97. doi:10.1016/j.molstruc.2008.03.002

Figure Captions:

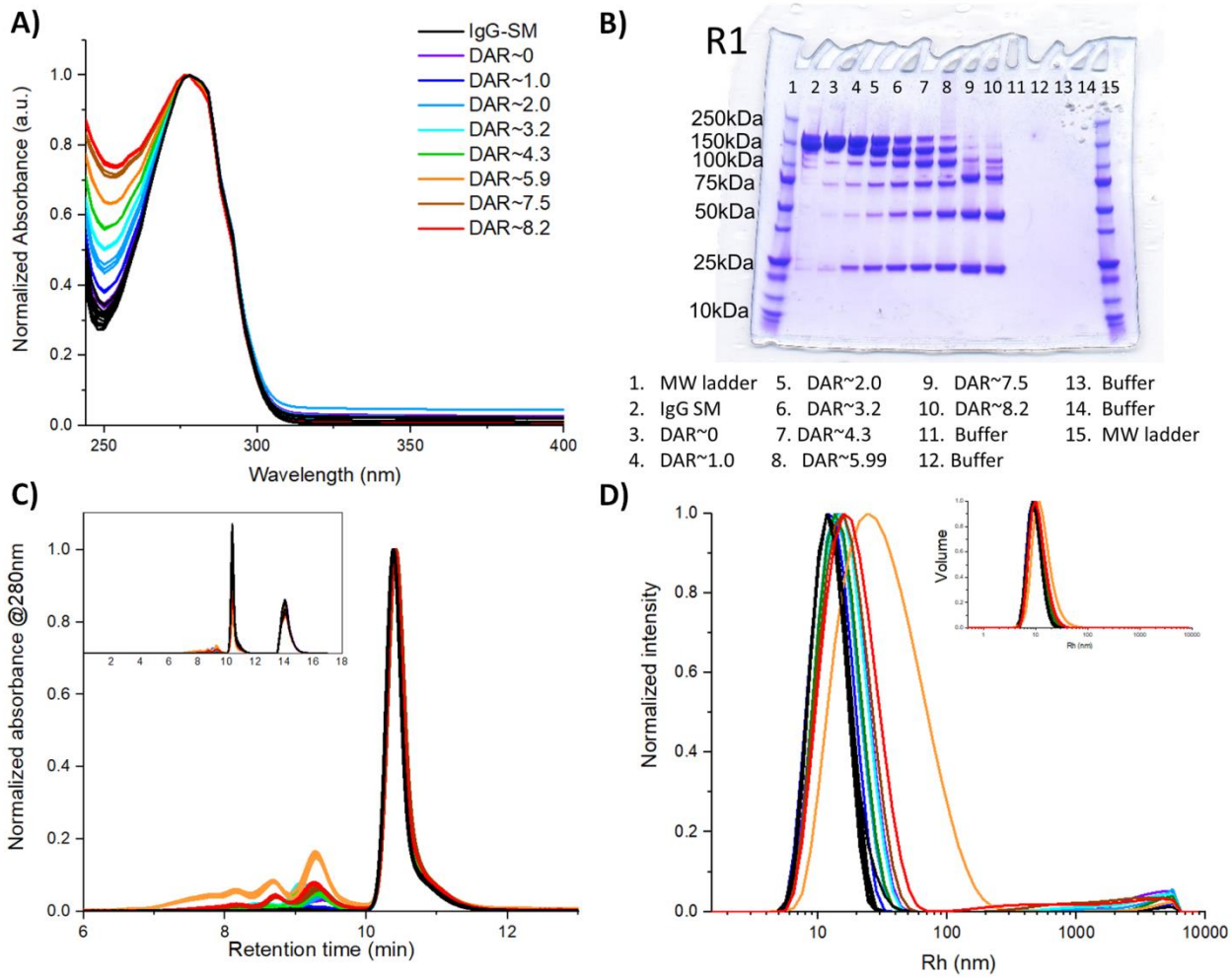

Figure 1: (A) Normalized absorbance spectra of purified products; (B) SDS-PAGE gels, Coomassie blue stained, of Pur-ADC samples (first reaction replicate only, see Figure S4, SI for replicate measurements); (C) Normalized SEC chromatograms; (D) normalized DLS intensity obtained from analysis of starting materials (IgG-SM) and purified products (Pur-ADC); The data shown is the mean of the triplicate reactions carried out for each condition.

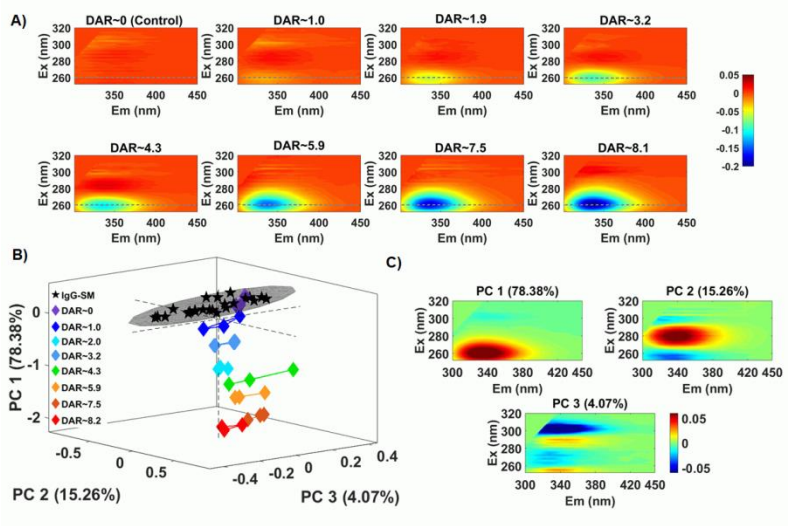

Figure 2: (A) Difference spectra (Pur-ADC – IgG SM) calculated using normalized $EEM_{||}$ spectra plotted over the 300 to 450 nm emission range (the dashed lines show the 260 nm excitation). The spectra used for calculation was the average from the triplicate reactions carried out for each reaction condition. ROBPCA, using Normalized $EEM_{||}$ data from the Pur-ADC and IgG SM sample set (n= 48); (B) scores and (C) loadings plots.

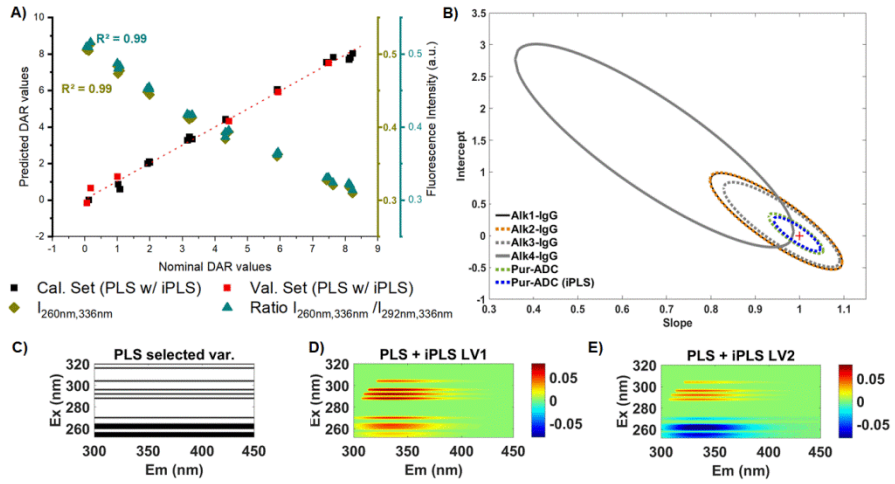

Figure 3: (A) Plots of nominal versus predicted DAR values from u-PLS modelling of all **Pur-ADC** samples after iPLS variable selection. Linear regression results of nominal DAR values vs intensity at $\lambda_{ex/em}$ 260/336nm (green) and ratio between λ_{ex} 260/336nm and 292/336nm (blue). (B) EJCR plot at 95% confidence level for the regression slope

and intercept (1,0) of predicted vs nominal DAR values of Pur-ADC. (C) Selected wavelengths (in black) after iPLS variable selection for models built with **Pur-ADC**. (D,E) LV1 and 2 loadings from u-PLS models built using Pur-ADC EEM data after variable selection.

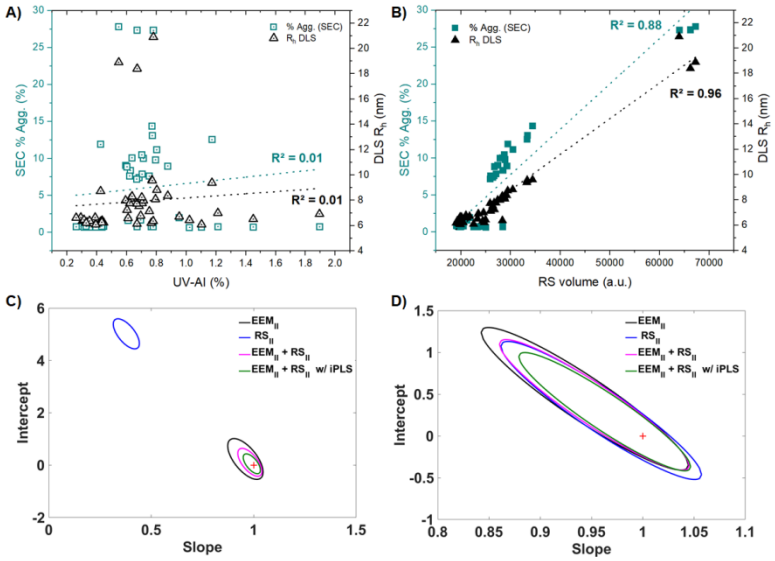

Figure 4: Scatter plots showing sample distribution, with % aggregation (as determined by SEC) and R_h and (DLS) measurements plotted against: (A) UV-AI, and (B) $RS_{||}$ volume measurements. Linear fits are included for reference. EJCR plots for u-PLS regression models (using SM and Pur-ADC sample sets and $RS_{||}$ and $EEM_{||}$ data) for prediction of: (C) %Aggregation (%Agg,), and (D) R_h values (main (small species) peak from distribution fit of the DLS data).

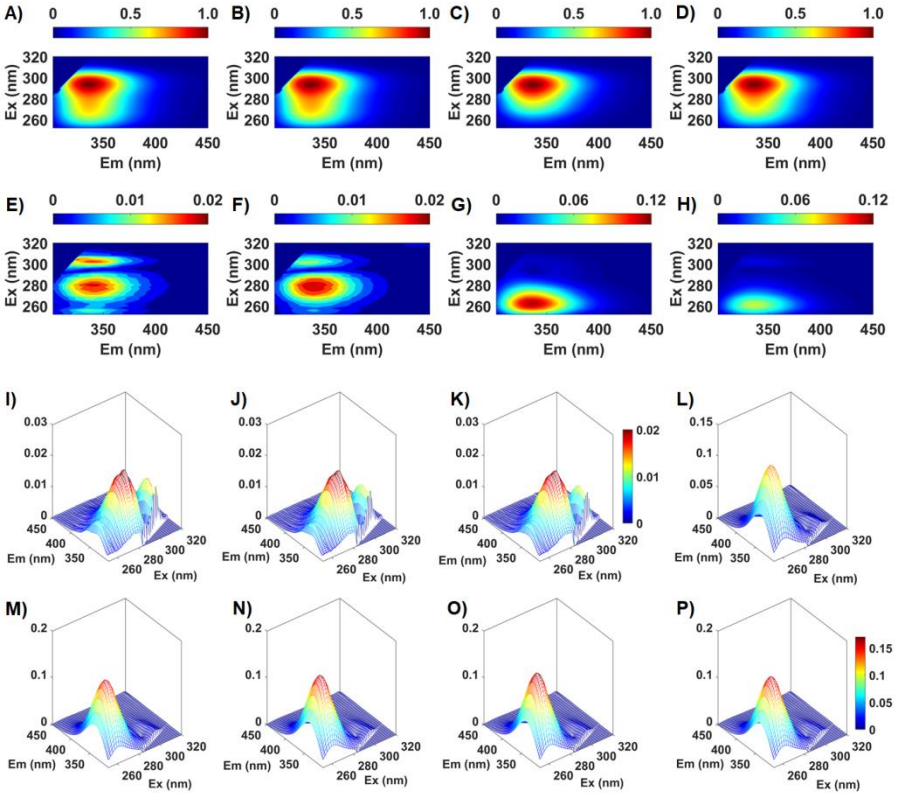

Figure 5: Rows 1 and 2: Mean (top) and Std.Dev (bottom) spectra calculated for IgG SM (A,E), Red-IgG (B,F), Alk-IgG (C,G), and Pur-ADC (D,H) showing the variance between the 24 reaction solutions in each of these four datapoints during the reaction. **Rows 3 and 4:** Cumulative Standard deviations calculated from addition of extra process step samples to the starting material sample set (n=24): (I) +Red1-IgG (n=48); (J) +Red2-IgG (n=72), (K) +Red3-IgG (n=96), (L) +Alk1-IgG (n=120), (M) +Alk2-IgG (n=144), (N) +Alk3-IgG (n=168), (O) +Alk4-IgG (n=192), and (P) +Pur-ADC (n=216). This shows the amount of signal variation available for modelling over the process, and how the scatter contribution decreases during the alkylation step. See Table S2, SI, for details of the sample sets.

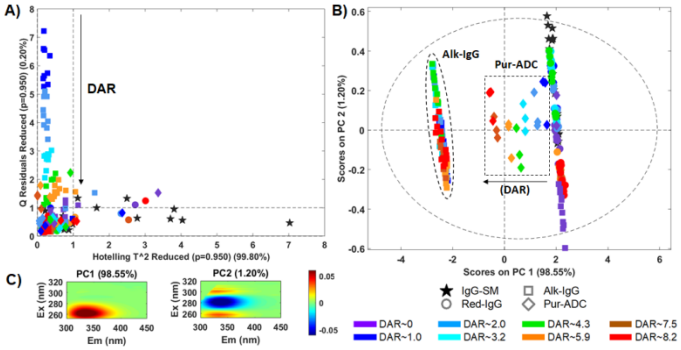

Figure 6: Results of ROBPCA analysis of $EEM_{||}$ dataset (IgG-SM+Red1,2,3-IgG+Alk1,2,3,4-IgG,Pur-ADC, n=216). (A) Q residuals vs Hoteling (outliers) plot, (B) PC1 vs PC2 scores; and (C) refolded loadings plots. The symbols represent the reaction stage (pentagram, circle, square and diamond for IgG-SM, Red-IgG, Alk-IgG, and Pur-ADC respectively) and colors the DAR of final Pur-ADC as indicated by the legend. The boundaries for Alk-IgG and Pur-ADC were included as a visual guide to show the two groups.

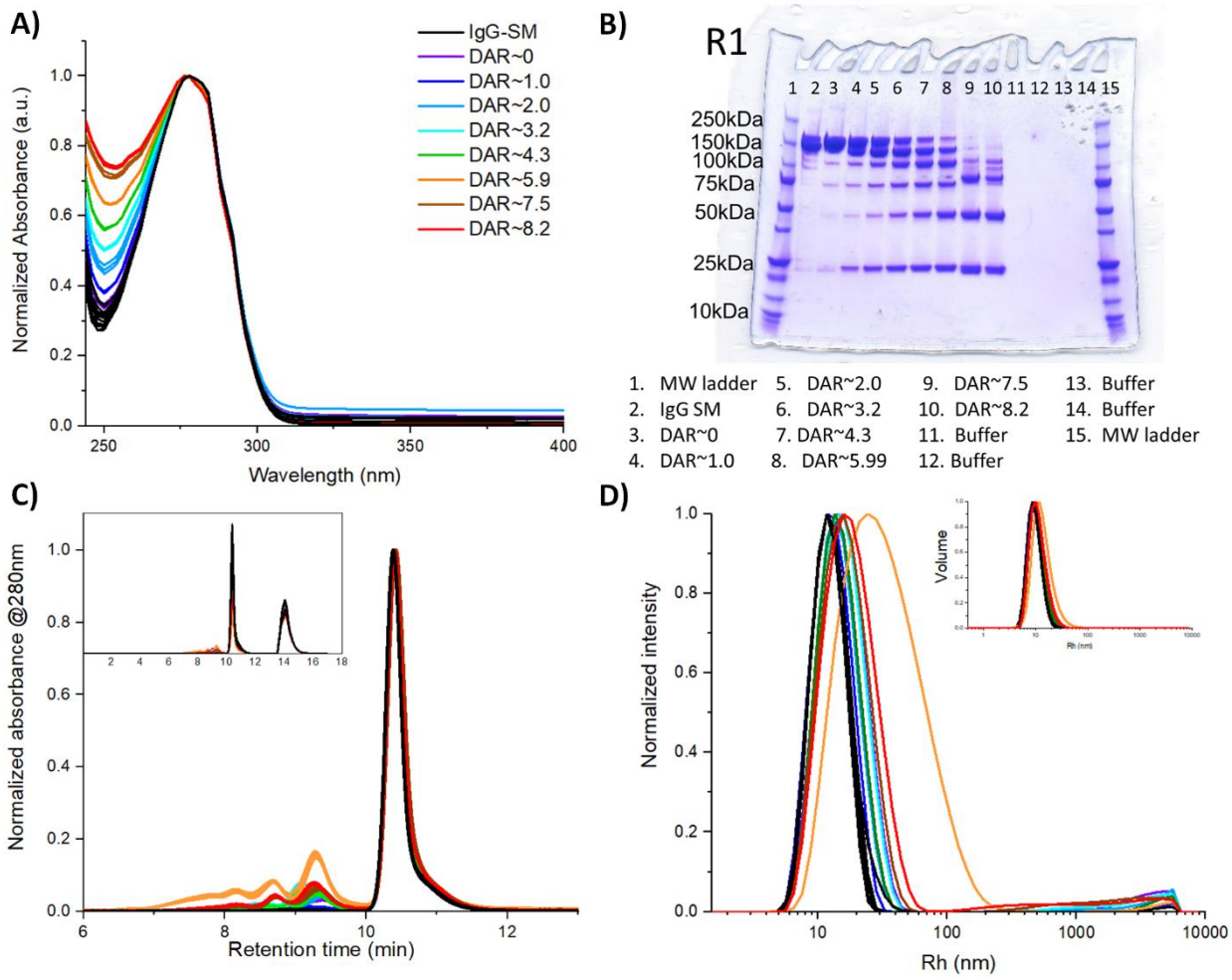

Figure 1:

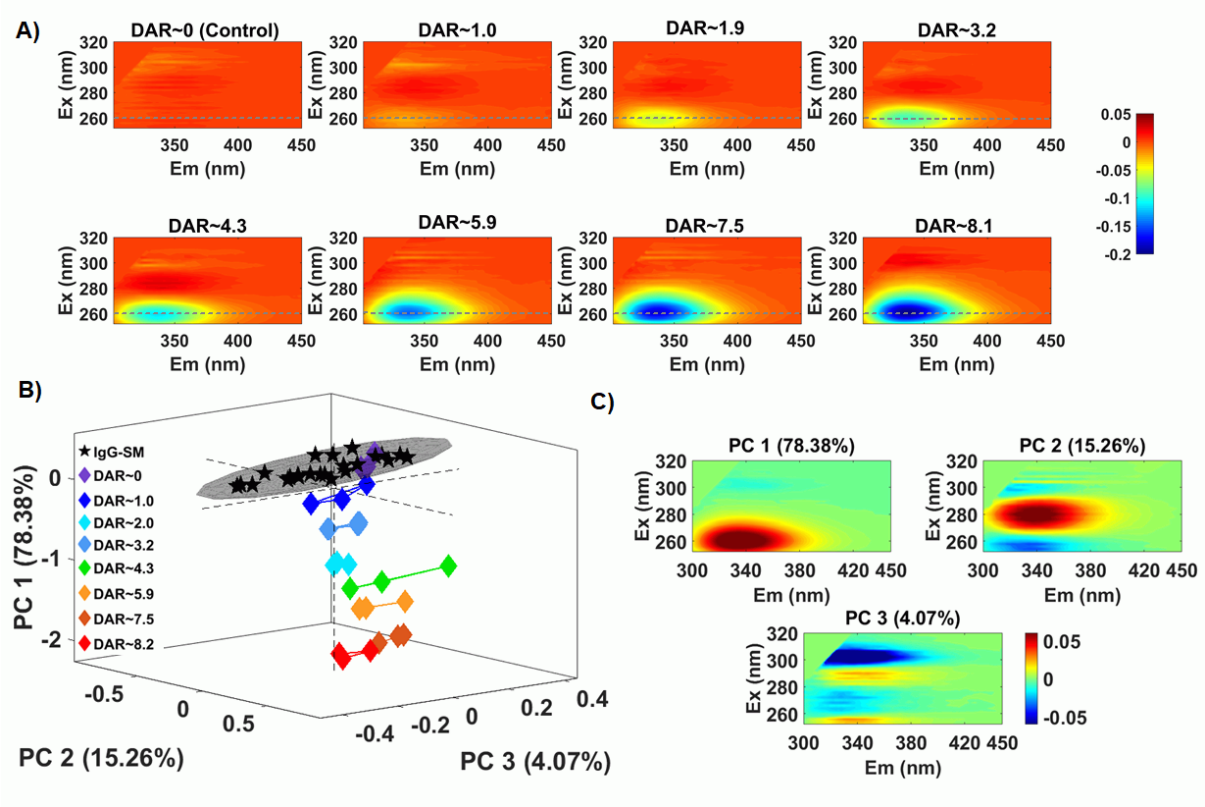

Figure 2:

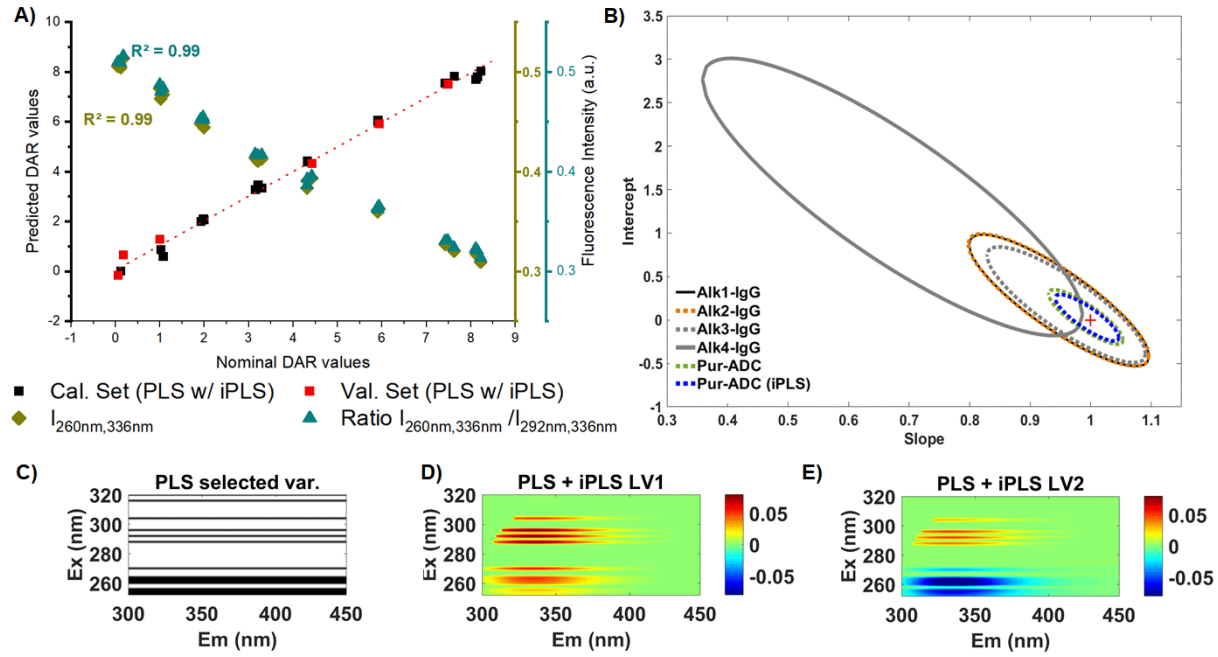

Figure 3:

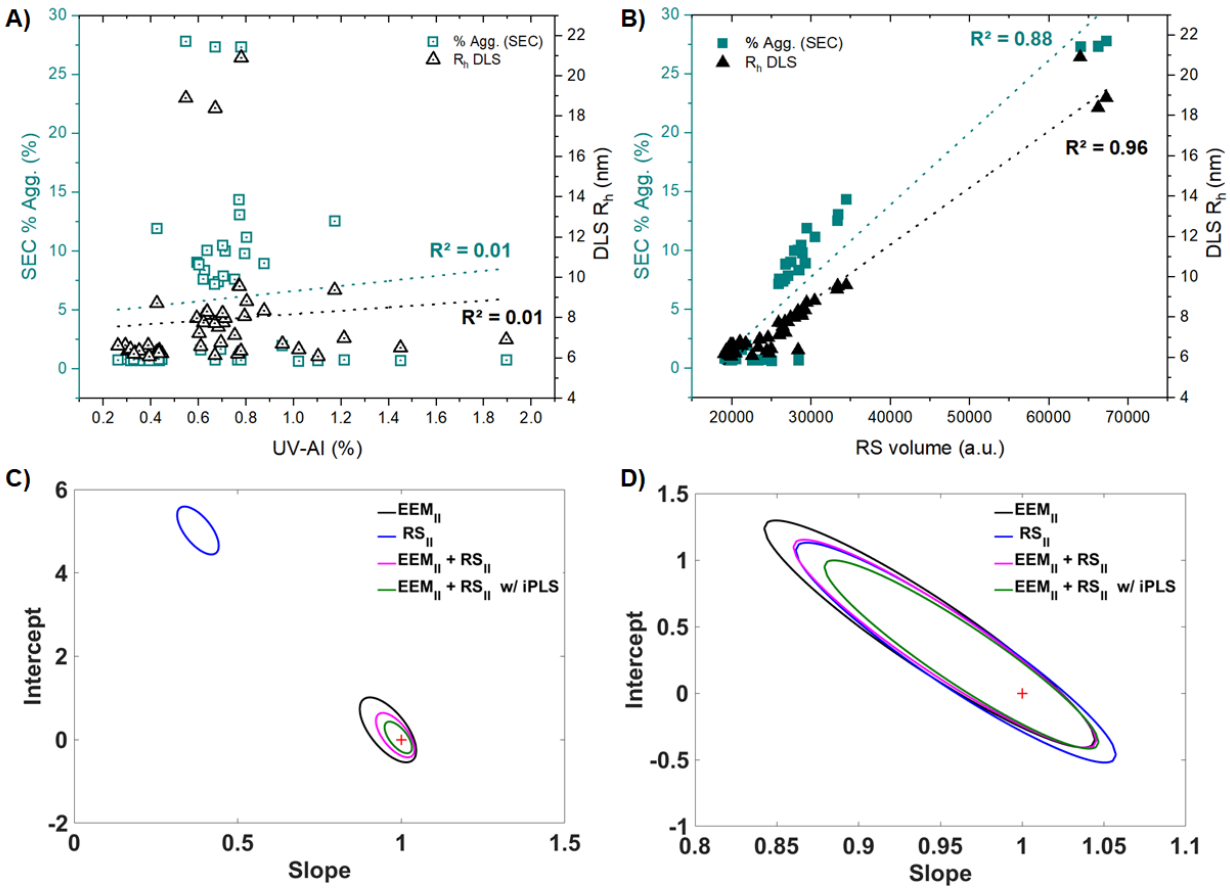

Figure 4:

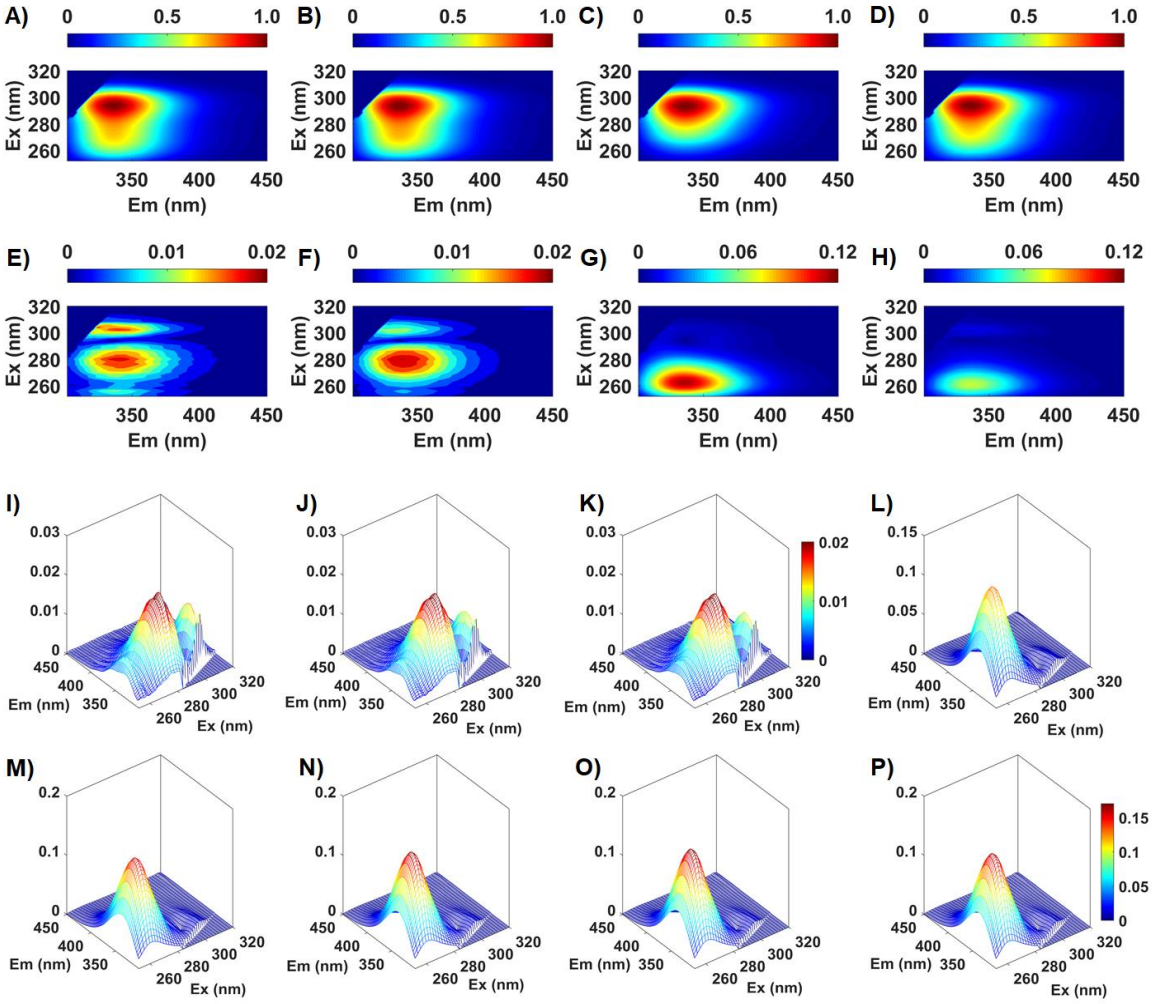

Figure 5:

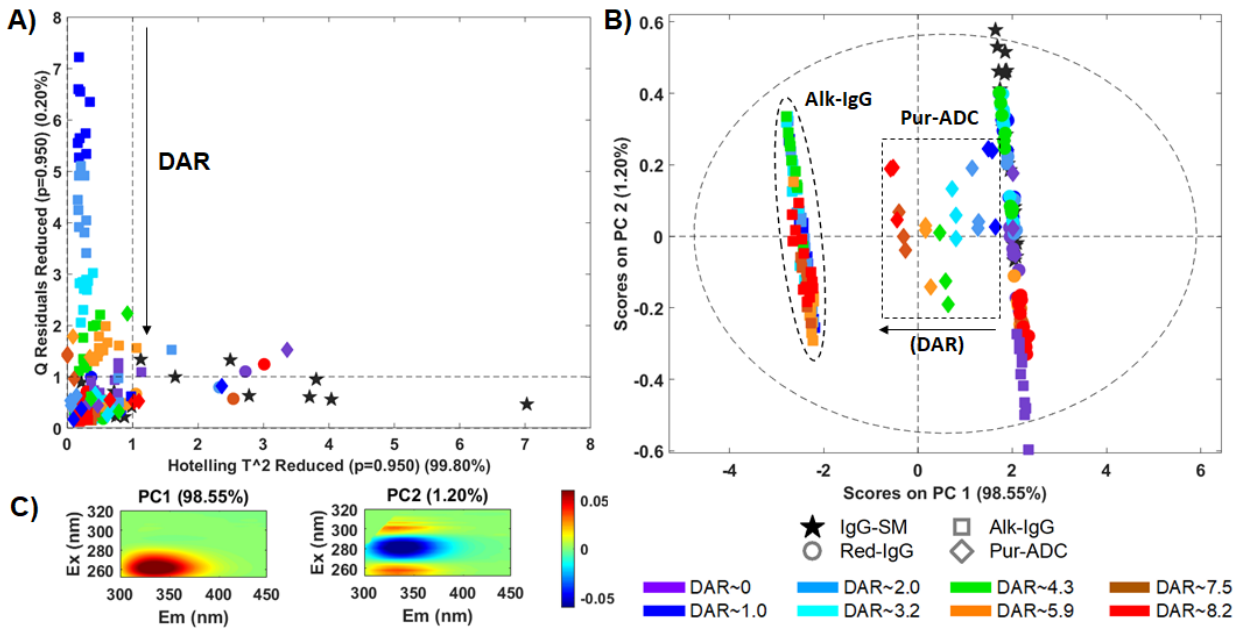

Figure 6:

Table 1: Average sample data: nominal and PLS predicted DAR, % of aggregates (from SEC), Hydrodynamic radius, R_h (from DLS), and Rayleigh Scatter (RS) volumes, see also Figures S5, SI. DAR was calculated from Pur-ADC absorbance spectra, according to the procedure given in the SI and PLS predicted DAR was obtained from u-PLS models of $EEM_{||}$ after iPLS variable selection (calibration and validation data were included). More DLS data (e.g., Z-avg.) is available in Table S3, SI.

[TCEP] (M excess)	DAR		% Aggregates (from SEC)		R_h (from DLS)		RS volume (from $EEM_{||}$)	
	Nominal	Predicted ($EEM_{||}$)	IgG-SM	Pur-ADC	IgG-SM	Pur-ADC	IgG-SM	Pur-ADC
0 Control	0.1±0.1	0.2±0.4	0.8±0.1	8.8±4.0	6.3 ± 0.2	8.2 ± 0.1	19,250±206	28,345±912
1.25	1.0±0.0	0.9±0.3	0.8±0.1	1.8±0.5	6.4 ± 0.4	6.7 ± 0.1	20,220±198	21,314±382
2.5	2.0±0.0	2.1±0.1	0.8±0.1	7.6±2.3	6.4 ± 0.2	7.5 ± 0.4	19,822±48	26,481±548
5.0	3.2±0.1	3.4±0.1	0.8±0.1	10.0±2.6	6.4 ± 0.1	8.1 ± 0.4	19,877±93	28,346±498
7.5	4.3±0.1	4.4±0.0	0.7±0.1	7.9±2.2	6.3 ± 0.1	7.6 ± 0.3	19,629±18	26,429±487
10	5.9±0.0	6.0±0.1	0.7±0.1	27.5±1.1‡	6.4 ± 0.1	19.4 ± 1.6‡	25,546±2559	65,798±1687

25	7.5±0.1	7.6±0.2	0.8±0.1	11.2±0.9	6.7 ± 0.4	8.6 ± 0.1	22,647±2448	29,523±862
50	8.2±0.1	7.9±0.2	0.8±0.1	13.3±1.0	6.2 ± 0.1	9.5 ± 0.3	23,888±1173	33,687±844

[‡]In addition to the high DAR, these samples had a long hold time during purification, which might explain the higher aggregation. [§]R_h was defined as the R_h calculated for the main peak (results are the average of three reactions measured 5×10 times).

Table 2: Summary of u-PLS DAR prediction results using normalized spectra of alkylation intermediates and Pur-ADC with and without iPLS variable selection. In all cases the total sample number was 24, which were split into calibration (n=18) and external validation (n=6) sets (the same samples in all cases)**.**

	Absorbance spectra				**pEEM**					
	Alk1-IgG	**Alk2-IgG**	**Alk3-IgG**	**Alk4-IgG**	**Alk1-IgG**	**Alk2-IgG**	**Alk3-IgG**	**Alk4-IgG**	**Pur-ADC**	
Var. Sel.	**-**	**-**	**-**		**-**	**-**	**-**	**-**	**-**	**iPLS**
RMSE Cal	0.49	0.48	0.53	0.91	0.61	0.61	0.53	1.53	**0.25**	0.21
RMSE CV	0.71	0.66	0.75	1.42	1.30	0.98	0.76	3.18	**0.29**	0.23
RMSE Pred (REP)	0.89 (28%)	0.91 (29%)	0.88 (28%)	1.72 (54%)	0.56 (18%)	0.68 (22%)	0.34 (11%)	1.15 (39%)	**0.19 (6%)**	0.25 (8%)
R^2 Cal	0.97	0.97	0.96	0.88	0.95	0.95	0.96	0.67	**0.99**	0.99
R^2 CV	0.93	0.94	0.92	0.73	0.82	0.88	0.92	0.11	**0.99**	0.99
R^2 Pred	0.94	0.94	0.94	0.90	0.96	0.97	0.99	0.90	**1.00**	0.99

Table 3: Summary of ROBPCA $EEM_{||}$ modelling results for: 1). all reaction/product samples, 2). only IgG-SM, 3). only reduction intermediates (Red-IgG), 4). combined model of IgG-SM and Red-IgG, 5). only alkylation intermediates (Alk-IgG); and 6). IgG-SM and Pur-ADC.

ROBPC	**All samples**	**IgG-SM +**	**Alk-IgG**[†]	**IgG-SM**	**Red-IgG**	**IgG-SM**

	(n=216)	Red-IgG (n=96)	(n=96)	(n=24)	(n=72)	and Pur-ADC (n=48)
1	98.55	91.65	71.42	73.29	91.12	78.38
2	1.20	2.87	21.50	18.93	2.68	15.26
3	0.06	1.46	2.99	1.07	1.71	4.07
4	-	-	0.49	-	-	0.44
Total variance	**99.81**	**95.98**	**96.41**	**93.29**	**95.51**	**98.15**

†This model did not include control samples, which were considered outliers in the model because of the absence of linker.

Table 4: Summary of u-PLS modelling results obtained for % of Aggregate and R_h quantification using the fluorescence signal from $EEM_{||}$, the $RS_{||}$ (not normalized), and the combined fluorescence and scatter signal. For u-PLS modelling EEM spectra were normalized to maximum intensity, EEM with RS were normalized to $\lambda_{ex/em}$ 294/336nm, which is a data point with high intensity value and low StDev.

	IgG SM + Pur-ADC (n=48, cal.=36/val.=12) †								**IgG SM + Red3-IgG+ Alk4-IgG +Pur-ADC (n=96, cal.=72 /val.=24)** †			
	% Agg. (from SEC)				**R_h (from DLS)**				**R_h**			
	$EEM_{||}$	**$RS_{||}$**	**$EEM_{||}$+ RS**		**$EEM_{||}$**	**$RS_{||}$**	**$EEM_{||}$+$RS_{||}$**		**$EEM_{||}$**	**$RS_{||}$**	**$EEM_{||}$+RS**	
			-	**iPLS**			**-**	**iPLS**			**-**	**iPLS**
RMSE Cal	1.39	4.63	0.94	0.67	0.74	0.70	0.67	0.57	1.42	0.70	0.51	0.46
RMSE CV	2.28	4.76	1.18	0.93	1.32	0.72	0.78	0.71	1.78	0.72	0.70	0.61
RMSE Pred	1.91 (31%)	4.86 (79%)	1.28 (21%)	1.13 (18%)	0.63 (9%)	0.59 (9%)	0.54 (7%)	0.47 (6%)	1.61 (21%)	0.81 (11%)	0.60 (8%)	0.49 (6%)
R^2 Cal	0.96	0.87	0.98	0.99	0.94	0.95	0.95	0.97	0.62	0.91	0.95	0.96
R^2 CV	0.89	0.88	0.97	0.98	0.82	0.95	0.94	0.95	0.42	0.90	0.91	0.93
R^2 Pred	0.94	0.90	0.99	0.99	0.97	0.98	0.99	0.99	0.67	0.91	0.97	0.97

† The same samples were used for calibration and prediction in each sample group to enable comparison between various measurements/parameters.